Chemical Science

ROYAL SOCIETY OF CHEMISTRY

EDGE ARTICLE

View Article Online
View Journal | View Issue

Cite this: *Chem. Sci.*, 2024, **15**, 2601

All publication charges for this article have been paid for by the Royal Society of Chemistry

Breaking the trade-off between capacity and stability in vanadium-based zinc-ion batteries†

Weikang Jiang,[ab] Kaiyue Zhu,*[bc] Weili Xie,[bc] Zhengsen Wang,[bd] Zuqiao Ou[bc] and Weishen Yang *[abcd]

Water in electrolytes is a double-edged sword in zinc-ion batteries (ZIBs). While it allows for proton insertion in the cathode, resulting in a significant increase in capacity compared to that of organic ZIBs, it also causes damage to electrodes, leading to performance degradation. To overcome the capacity-stability trade-off, organic solvents containing a small amount of water are proposed to mitigate the harmful effects of water while ensuring sufficient proton insertion. Remarkably, in a $Zn(OTf)_2$ electrolyte using 8% H_2O in acetonitrile as the solvent, $Zn||(NH_4)_{0.5}V_2O_5\cdot 0.5H_2O$ exhibited a capacity as high as 490 mA h g^{-1} at a low current (0.3 A g^{-1}), with a capacity retention of 80% even after 9000 cycles at high current (6 A g^{-1}), simultaneously achieving the high capacity as in pure aqueous electrolytes and excellent stability as in organic electrolytes. We also found that the water content strongly impacts the kinetics and reversibility of ion insertion/extraction and zinc stripping/plating. Furthermore, compared to electrolytes with pure acetonitrile or H_2O solvents, electrolytes with only 8% H_2O in acetonitrile provide higher capacities at temperatures ranging from 0 to −50 °C. These discoveries enhance our understanding of the mechanisms involved in ZIBs and present a promising path toward enhancing electrolyte solutions for the creation of high-performance ZIBs.

Received 26th October 2023
Accepted 4th January 2024

DOI: 10.1039/d3sc05726g

rsc.li/chemical-science

Introduction

Zinc-ion batteries (ZIBs) have gained increasing attention for their advantages of high power density, low cost, and environmental friendliness, making them highly promising for various applications.[1–5] However, ZIBs in organic electrolytes deliver a low capacity due to the large charge-to-radius ratio of zinc ions, while a substantial increase in capacity is achieved for ZIBs in water-based electrolytes owing to the "lubricating" effect of water molecules and the capacity contribution of proton insertion into cathodes despite the unsatisfactory long-term stability.[6–13] Therefore, achieving high capacity and excellent stability simultaneously in ZIBs is crucial for enhancing their competitiveness.

Many studies have demonstrated that water plays a crucial role in the performance of cathodes in ZIBs.[11,14–16] For example, our previous investigation utilized density functional theory (DFT) calculations to reveal that the presence of water in interlayers plays a crucial role in creating a smooth electrostatic environment between V_2O_5 sheets.[17] This facilitates facile Zn^{2+} diffusion due to the combined effects of "charge shielding" and the interaction between O in H_2O and Zn^{2+}. A recent study by Lu *et al.* similarly highlighted the significant impact of the interlayer water content in $V_2O_5\cdot nH_2O$ on the capacity.[18] Drawing from our previous work, we noted that water from electrolytes could enter the interlayers of some layered vanadium oxides, such as $V_2O_5\cdot nH_2O$, $Zn_{0.1}V_2O_5\cdot nH_2O$ and $MV_6O_{16}\cdot nH_2O$ (M = Na, K, NH_4^+).[15,19,20] Consequently, the water content in the electrolyte also plays a crucial role in improving the performance. Additionally, the presence of water serves to supply protons for insertion into the positive electrode interlayer.[21–24] Due to their small size and low migration energy barriers, protons can rapidly migrate within the positive electrode phase and fully utilize more active sites, increasing the capacity and approaching the theoretical capacity of the positive electrode material. For example, both Nazar's team and our team showed that the presence of water as a solvent can increase the interlayer distance of $V_2O_5\cdot nH_2O$ and $V_3O_7\cdot nH_2O$ from 10 Å to 13 Å.[8,15,16,19] In Zn^{2+}-based electrolytes that use pure acetonitrile as a solvent, the capacity of $V_3O_7\cdot H_2O$ is approximately 150 mA h g^{-1} since only zinc ions undergo reversible insertion/extraction during charge and discharge. However, when the electrolyte is switched to a water-based electrolyte, the capacity increases to 400 mA h g^{-1} due to proton insertion.[8] Currently, proton insertion is achievable in a wide range of positive electrode materials, including manganese-based oxides, vanadium-

[a]*Department of Chemical Physics, University of Science and Technology of China, Hefei, Anhui 230026, China. E-mail: yangws@dicp.ac.cn*

[b]*State Key Laboratory of Catalysis, Dalian Institute of Chemical Physics, Chinese Academy of Sciences, Dalian, 116023, China. E-mail: zky218@dicp.ac.cn*

[c]*University of Chinese Academy of Sciences, Beijing, 100049, China*

[d]*School of Chemistry, Dalian University of Technology, Dalian, 116024, China*

† Electronic supplementary information (ESI) available. See DOI: https://doi.org/10.1039/d3sc05726g

based oxides, Prussian blue analogs, and organic compounds, thereby enhancing their capacity.[25–32] Among these cathode materials for ZIBs, manganese-based oxides suffer from slow kinetics, manganese dissolution, and structural collapse, whereas Prussian blue and organic materials have lower specific capacities.[30,33,34] In contrast, vanadium-based materials have high theoretical specific capacities (*e.g.*, V_2O_5 can reach 588 mA h g^{-1}) and large interlayer spacing (approximately 13 Å), exhibiting excellent rate performance and hence garnering extensive attention from researchers.[35–37] As a result, several ideal vanadium-based positive electrode materials have been developed, such as $Zn_xV_2O_5 \cdot nH_2O$, $(NH_4)_2V_{10}O_{25} \cdot nH_2O$ (NVO), $ZnV_6O_{16} \cdot 8H_2O$, and $Na_2V_6O_{16} \cdot 8H_2O$.[15,16,19,38–43] Therefore, as a proof-of-concept, we used NVO to represent vanadium-based cathodes in this work.

However, although water molecules can increase the capacity of a cathode, water also poses certain problems. Proton insertion into the cathode releases hydroxide ions that react with zinc ions in the electrolyte, leading to the formation of layered byproducts such as zinc sulfate hydroxides and zinc hydroxides. For example, in an aqueous zinc sulfate electrolyte, proton insertion leads to the formation of $Zn_4(SO_4)(OH)_6 \cdot nH_2O$ nanoflakes on the cathode surface, and the reversibility of these nanoflakes directly impacts the cycling stability of ZIBs.[15,22,29] In addition, water molecules cause dissolution and phase transition problems in vanadium-based materials, leading to poor long-term cycling performance.[44,45] Apart from the negative effects on the cathode, the presence of water molecules in the electrolyte of zinc-ion batteries also leads to the hydrogen evolution reaction and the generation of a large amount of byproducts on the negative electrode, reducing the reversibility of the zinc negative electrode and the utilization of zinc.[43,46,47]

In brief, while water has a positive role in increasing the capacity, excessive water is also the main cause of instability in the vanadium-based cathode and zinc anode, thus limiting the long-term cycling performance of aqueous ZIBs in practical applications. Therefore, achieving a balance between the roles of water in the capacity and stability of ZIBs necessitates precise control of the water content and the solvation structures surrounding Zn^{2+} ions.[48,49] To this end, super-concentrated solvent-in-salt electrolytes (SISEs) such as 30 m $ZnCl_2$ and 1 m $Zn(TFSI)_2$ + 20 m LiTFSI have been explored; these electrolytes can reduce the water content and modify the solvation structures of Zn^{2+} ions by replacing water molecules with $TFSI^-$ ions.[50–54] However, the susceptibility of Cl^- to oxidation and the high cost of these SISEs limit their practical application. Although electrolyte additives such as methanol, *N*-methyl-2-pyrrolidone, dimethyl sulfoxide, and polyacrylamide have been investigated for their ability to modify the solvation structure of Zn^{2+} ions in dilute solutions, the quantity of these additives is much lower than that of water, and their effectiveness in mitigating side reactions on the Zn anode is limited.[43,55–66] Moreover, the water content in the electrolyte remains excessively high for the cathode and a systematic exploration of the potential impact of these additives on the cathode is lacking.

Herein we propose the use of organic electrolytes containing a small amount of water to enable sufficient proton insertion to increase the capacity while suppressing the harmfulness of the electrolyte on both the cathode and anode. Our study demonstrated that even a small quantity of water can significantly enhance the capacity of ZIBs, approaching that of aqueous ZIBs. The water content in electrolytes strongly affects the solvation structures surrounding Zn^{2+} as well as the physical properties (such as ionic conductivity, the electrochemical stability window, and anti-freezing properties) of electrolytes. Systematic experiments reveal that the water content and organic solvents have a significant impact on the stability of the cathode material and Zn anode, together with the reversibility of ion insertion/extraction and zinc plating/stripping, which ultimately determine the long-term cycling stability of ZIBs. Additionally, we found that electrolytes using AN with 8% H_2O as a solvent provide higher capacities at low temperatures ranging from 0 to −50 °C than electrolytes containing either pure AN or H_2O alone. Therefore, a thorough study of the effects of the water content on the Zn anode and V-based cathodes not only enhances the understanding of ZIB mechanisms but also provides important guidance for achieving excellent performance of ZIBs through electrolyte design.

Results and discussion

The critical role of water content in electrolytes on the performance of zinc-ion batteries

To investigate the impact of electrolytes on capacity and long-term cycling stability, commercial zinc foil and conventional $(NH_4)_{0.5}V_2O_5 \cdot 0.5H_2O$ (NVO) (Fig. S1†) were chosen as the anode and cathode (active mass loading of ~1 mg cm^{-2}), respectively, for zinc-ion batteries (ZIBs). The 1 M $Zn(OTf)_2$ electrolyte using acetonitrile (AN) with minimal H_2O content as the solvent was chosen as an example for the following reasons. To precisely assess the influence of water, selecting a solvent that does not introduce protons is of utmost importance. Consequently, we opted for AN as the organic solvent due to its excellent solubility and aprotic characteristics. Additionally, $Zn(OTf)_2$ was selected because of its anhydrous nature and high solubility in various mixtures of water and AN solvents. $ZnSO_4$ and $Zn(OTf)_2$ are widely adopted as electrolytes for ZIBs due to their superior performance compared to other electrolytes such as $ZnCl_2$, $Zn(OAc)_2$, and $Zn(NO_3)_2$.[5] However, it is important to note that $ZnSO_4$ is not available in an anhydrous form. Furthermore, hydrous $ZnSO_4$ (such as $ZnSO_4 \cdot H_2O$ or $ZnSO_4 \cdot 7H_2O$) cannot be dissolved in AN to achieve a 1 M concentration due to its low solubility in aprotic solvents. Therefore, $Zn(OTf)_2$ was selected as the solute for the investigations. Finally, the electrolytes used were 1 M $Zn(OTf)_2$ in AN with varying amounts of H_2O (0%, 5%, 8%, 15%, and 100% water volume ratios in solution), denoted as E-*x*H_2O (*x* represents the volume ratios of water in solution).

As shown in Fig. 1a, S2 and S3,† a capacity of 110 mA h g^{-1} was obtained in the water-free electrolyte (pure AN), while there was a sharp increase to 350 mA h g^{-1} in 5% water and 475 mA h g^{-1} in 8% water, followed by a stable capacity of 475 mA h g^{-1} with further increases in the water content beyond

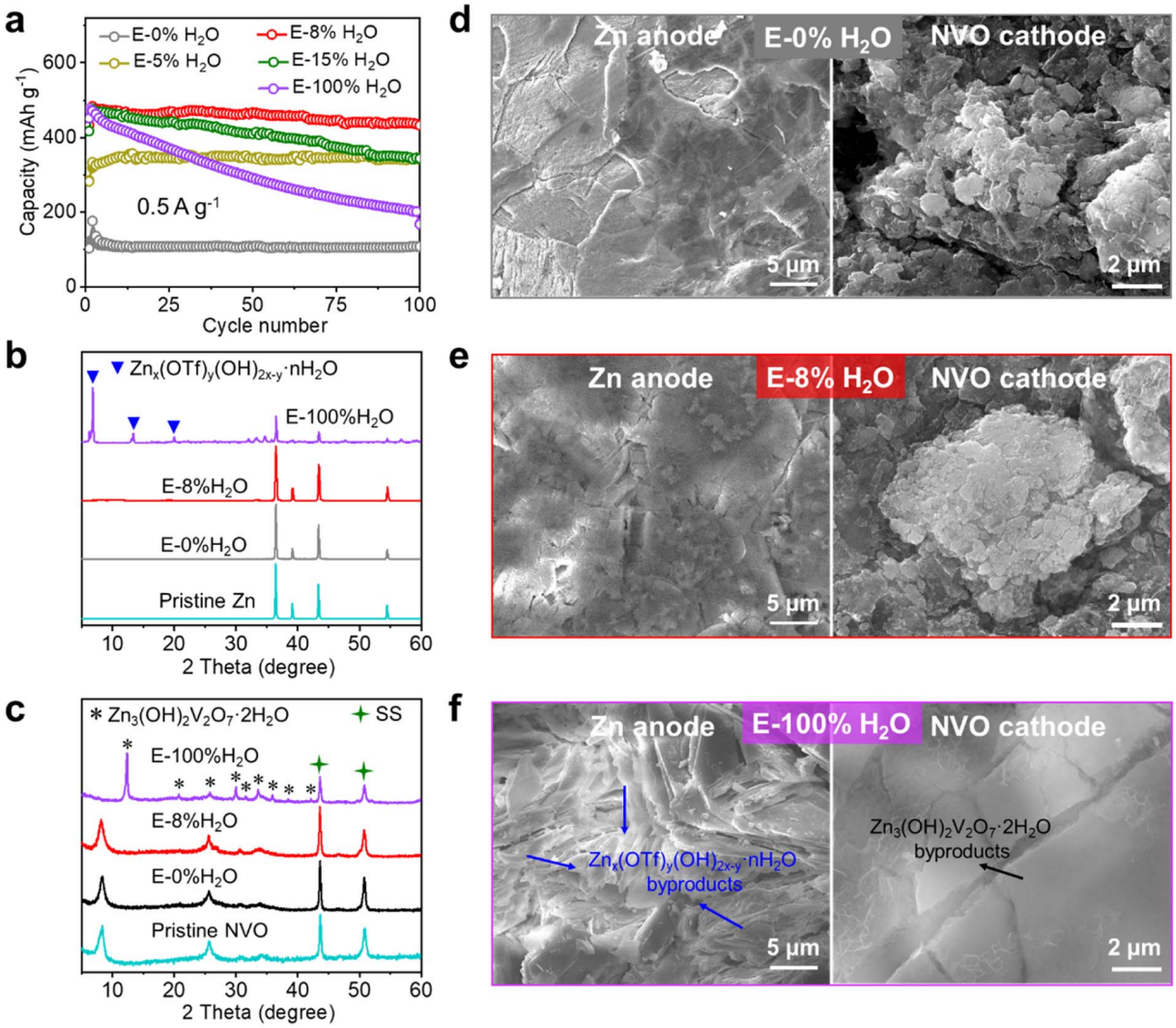

Fig. 1 Comparison of Zn||NVO in 1 M $Zn(OTf)_2$ using AN solvents with various H_2O contents. (a) The cycling performance at 0.5 A g^{-1}; X-ray diffraction (XRD) patterns of (b) Zn anodes and (c) NVO cathodes at pristine states and after 100 cycles at 5 A g^{-1} in various solvents; scanning electron microscopy (SEM) images of Zn anodes and NVO cathodes after 100 cycles at 5 A g^{-1} in 1 M $Zn(OTf)_2$ using AN solvents with various H_2O contents: (d) pure AN (E-0% H_2O), (e) 8% water in AN (E-8% H_2O), and (f) pure water (E-100% H_2O).

8%, even up to 100% H_2O. These results indicate that only a small amount of water contributes greatly to the capacity of ZIBs using $Zn(OTf)_2$ electrolytes in AN with different amounts of H_2O. This discovery is noteworthy, as it is the first to demonstrate that water in conventional aqueous electrolytes is far too excessive for achieving the highest capacity of cathodes. Moreover, Zn||NVO cells in electrolytes with less than 8% H_2O content exhibit excellent cycling performances, while the cycling stability of Zn||NVO was found to decrease as the water content in the electrolytes increased beyond 8% (15%, 100%). Similar changes in capacity and cycling stability with varying water contents (see Fig. S4†) were observed even at a high current density (5 A g^{-1}). The above significant effects of water content on capacity and cycling stability underscore the importance of controlling the water content in the electrolyte for optimal performance. Fig. 1b–f and S5† reveal that electrolytes strongly affect the deposition morphology of Zn anodes and the reversibility of NVO cathodes. After 100 cycles at 0.5 A g^{-1} in E-0% H_2O and E-8% H_2O, the Zn anode has a smooth surface and no byproducts, and the NVO cathode retains its well-maintained morphology without any byproducts. Conversely, when using E-100% H_2O, the Zn anode has a rough surface and a significant amount of $Zn_x(OTf)_y(OH)_{2x-y}\cdot nH_2O$ (ZOT), while the NVO cathode shows the presence of $Zn_3(OH)_2V_2O_7\cdot 2H_2O$ (ZVO) with large nanoplates.[44,67] After cycling NVO in E-100% H_2O, the marked decrease of NVO peak intensity and the large increase in $Zn_3(OH)_2V_2O_7\cdot 2H_2O$ peak intensity (Fig. 1c) demonstrated the dissolution of NVO and its transformation into $Zn_3(OH)_2V_2O_7\cdot 2H_2O$ (inactive for storing Zn^{2+}), thus leading to a significant decrease in capacity during cycling.[44,45]

Consequently, the capacity of E-0% H_2O is notably low due to the sole insertion of Zn^{2+}. However, the capacity increases with increasing water content from 0% to 8%, which is attributable

to the increased availability of H^+-insertion. Beyond 8% water content, zinc-ion batteries maintain their highest capacity because there is an excess of H^+ for insertion into the cathode. Nevertheless, the excessive use of water leads to corrosion of the Zn anode and dissolution of vanadium-based cathodes, thus resulting in diminished long-term cycling stability. Ultimately, at a water content of 8%, coin-type cells with a cathode mass loading of 1 mg cm^{-2} achieved the highest capacity and outstanding stability. Additionally, Fig. S6† shows that similar effects of water content on capacity and cycling performance are also observed for Zn||NVO when utilizing electrolytes with 1 M $Zn(OTf)_2$ in methanol and dimethyl formamide with varying amounts of H_2O.

The effects of water content on the physical properties of electrolytes

As AN and H_2O are miscible, no delamination was observed in the 1 M $Zn(OTf)_2$ electrolyte with water contents ranging from 0% to 100% (Fig. S7†). Fig. 2a shows that the ionic conductivity slightly decreases from 21.3 to 19.6 mS cm^{-1} with increasing H_2O content from 0% to 5% but gradually increases with increasing H_2O content from 8% to 100%. E-100% H_2O has the highest ionic conductivity (67.4 mS cm^{-1}), while E-5% H_2O has the lowest ionic conductivity (17.5 mS cm^{-1}) among all the electrolytes studied. This change in conductivity may be attributed to the alteration of solvation structures around Zn^{2+} as the H_2O content varies. Considering the substantial impact of ionic conductivity on the IR drop, it is important to highlight that the IR drop in zinc-ion batteries in 1 M $Zn(OTf)_2$ using AN solvent with various water contents is negligible, even at 5 A g^{-1} (approximately 2 mV), indicating the adequacy of the ionic conductivities. Moreover, the comparable capacities of E-8% H_2O and E-100% H_2O in Fig. 1a reinforce the notion of ample conductivity. At the same high Zn^{2+} concentration (1 M), the ionic conductivity bears no direct correlation with cycling stability, as the latter is influenced primarily by the stability and reversibility of the electrodes. Therefore, when the ionic conductivity reaches a sufficient level, its impact on performance, including capacity and cycle life, becomes negligible.

The Fourier transform infrared (FTIR) spectra in Fig. 2b and S8† reveal interesting insights into the solvation structures in $Zn(OTf)_2$ electrolytes with varying water contents. As $Zn(OTf)_2$ salts were dissolved in AN, the characteristic peak at 2293 cm^{-1}, which corresponds to the vibration of the –C≡N bond of AN, shifted to a low wavenumber and a peak at 2316 cm^{-1} appeared,

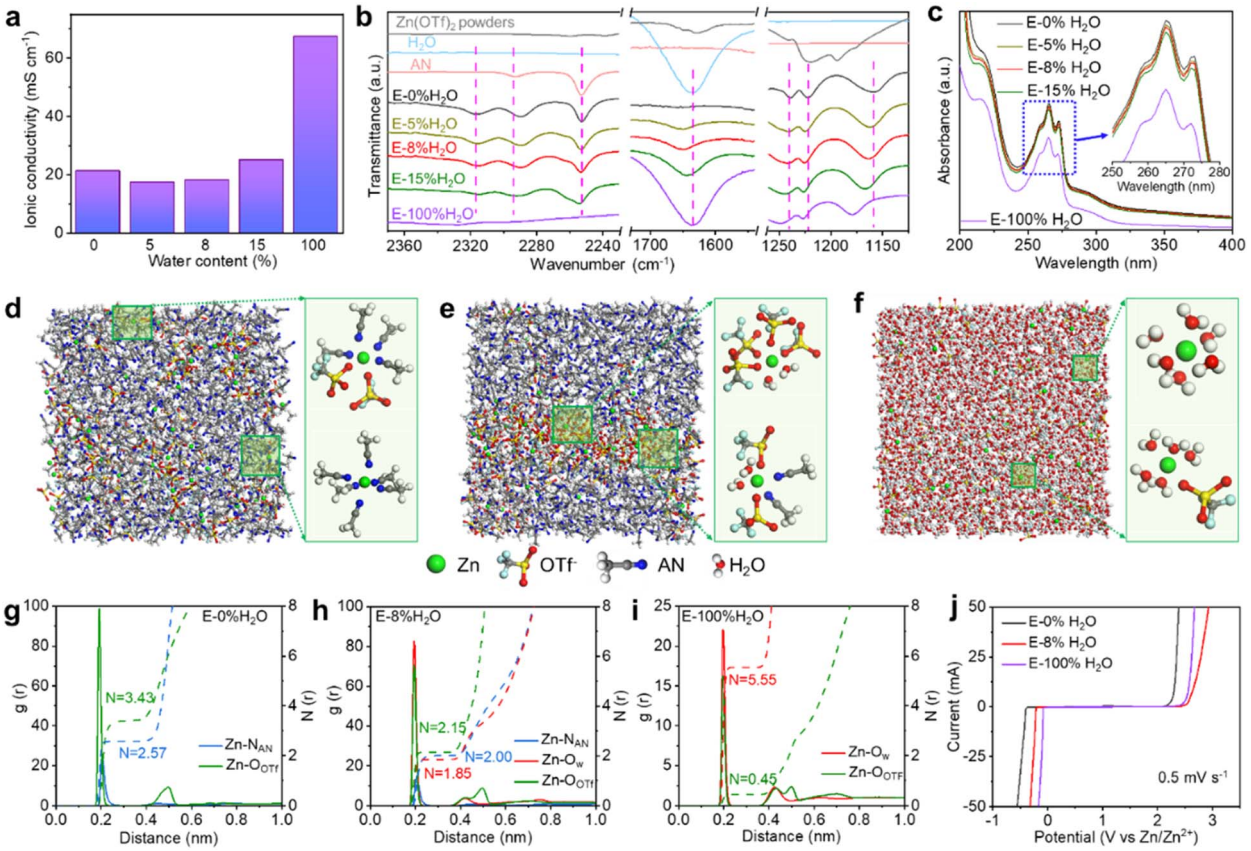

Fig. 2 Comparison of $Zn(OTf)_2$ electrolytes in AN with various H_2O contents. (a) The ionic conductivities, (b) FT-IR spectra and (c) UV-vis spectra for $Zn(OTf)_2$ electrolytes in AN with various H_2O contents. MD simulation snapshots of (d) E-0% H_2O, (e) E-8% H_2O, and (f) E-100% H_2O. RDFs and the corresponding average coordination numbers of (g) E-0% H_2O, (h) E-8% H_2O, and (i) E-100% H_2O. (j) The electrochemical stability windows of $Zn(OTf)_2$ electrolytes in AN with various H_2O contents (working electrode: stainless steel foil; counter electrode: Zn foil; reference electrode: Zn foil).

indicating the coordination of AN to Zn^{2+}.[68] The intensity decrease of the peak at 2316 cm^{-1} with increasing water content suggested a decrease in the coordination number of AN to Zn^{2+}. Similarly, the characteristic peaks at 1228, 1190, and 1052 cm^{-1} corresponding to the $(OTf)^-$ ions shift significantly after dissolution in AN with varying water contents, indicating the coordination of $(OTf)^-$ to Zn^{2+} in the solution.[69] The shift to a high wavenumber with increasing water content indicates a decrease in the coordination number of $(OTf)^-$ around Zn^{2+}. The presence of H_2O in the electrolyte solution is also evident from the strengthened O–H bending vibration peak at 1630 cm^{-1} and O–H stretching (~3300 cm^{-1}).[70] In addition, the UV-vis spectra of electrolytes with varying water contents in Fig. 2c show a gradual decrease in the adsorption peaks at 215 nm and 259–272 nm, corresponding to metal-to-ligand electron transfer (n–π*).[71,72] This decrease is likely due to changes in the solvation structures around Zn^{2+} with increasing water content in the electrolytes. It is important to note that the UV-vis spectra in Fig. 2c were obtained by excluding the solvent absorbance of water and AN.

To gain a deeper understanding of the Zn^{2+} solvation structures and the distribution of neighboring molecules, molecular dynamics (MD) simulations were performed. As shown in Fig. 2d, the MD simulations reveal that the $Zn(OTf)_2$ electrolyte prepared with pure AN (E-0% H_2O) consists mainly of $[Zn(AN)_6]^{2+}$ and $[Zn(AN)(OTf)_5]^{3-}$ aggregates due to the strong electrostatic interaction between Zn^{2+} and $(OTf)^-$ ions. Upon adding up to 8% H_2O, some $(OTf)^-$ around Zn^{2+} are replaced by water, which mainly results in the formation of $[Zn(H_2O)_2(OTf)_4]^{2-}$ and $[Zn(H_2O)_2(AN)_2(OTf)_2]$ in E-8% H_2O (Fig. 2e). In contrast, in the $Zn(OTf)_2$ electrolyte using pure H_2O (E-100% H_2O), the Zn^{2+} ions are coordinated by six H_2O molecules or five H_2O molecules and one $(OTf)^-$ ion (Fig. 2f). The corresponding radial distribution functions (RDFs) and coordination number distribution functions were further obtained (see Fig. 2g–i). In E-0% H_2O, the sharp $Zn–N_{AN}$ peak and $Zn–O_{OTf}$ peak at ~2.1 Å indicate a structured arrangement of 3.4 AN and 2.6 $(OTf)^-$ on average around Zn^{2+} ions in the solvation shell. On the other hand, in E-8% H_2O, the Zn^{2+} solvation shell is occupied by an average of 2 AN, 2.2 $(OTf)^-$ and 1.8 H_2O, while in E-100% H_2O, the Zn^{2+} solvation shell is occupied by 0.5 $(OTf)^-$ and 5.5 H_2O on average. Notably, the calculated diffusion coefficient of Zn^{2+} in E-8% H_2O is lower than that in E-0% H_2O and E-100% H_2O (Fig. S9†), which explains the lower ionic conductivity of E-8% H_2O. Overall, the solvation structure of Zn^{2+} is strongly affected by the water content in the electrolyte.

Fig. 2j demonstrates that the plating of Zn^{2+} and the stability of the electrolyte are significantly influenced by the water content. Compared to pure aqueous electrolytes, reducing the water content leads to a notable decrease in the Zn^{2+} plating potential, promoting uniform Zn^{2+} nucleation. Simultaneously, the potential for water oxidation increases, thereby enhancing the overall stability of the electrolyte. It is worth noting that the lowest plating potential is achieved in E-0% H_2O, but the observed easy oxidation in the E-0% H_2O electrolyte is likely a consequence of stainless steel (SS) oxidation in AN-based electrolytes (as shown in Fig. S10†).[73] The choice of SS as the working electrode is driven by the consideration that ZIBs are typically assembled in 2032 coin cells made of SS. The addition of some water to AN helps mitigate the leaching of ions from SS, resulting in a higher onset potential for oxidation. However, as the water content further increases to E-100% H_2O, water oxidation becomes even easier compared to E-8% H_2O. Thus, there is a delicate balance between achieving favorable Zn^{2+} plating conditions and ensuring the stability of the electrolyte when adjusting the water content.

The effects of water content on cathodes

The solvation structure of Zn^{2+} has a significant impact on the material's stability, kinetics and reversibility of ion insertion/extraction in the cathodes. To investigate the stability of the cathode materials in the electrolytes, NVO cathodes were immersed in electrolytes with varying water contents (E-0% H_2O, E-8% H_2O, and E-100% H_2O) for 10 days, after which the resulting changes were analysed. The E-100% H_2O solution turned pale yellow, indicating the dissolution of NVO, while the E-0% H_2O and E-8% H_2O solutions remained colourless as shown in Fig. 3a and S11a,† well explaining why there were no ZVO byproducts in E-0% H_2O and E-8% H_2O after 100 cycles (Fig. 1c–e). It should be noted that the crystal structures and morphologies in the three electrolytes (Fig. S11b and S12†) were still well-maintained in the electrolytes, suggesting that no phase transformation occurred during immersion. These results indicate that decreasing the water content can reduce the dissolution of the cathode, thereby enhancing the static stability.

The discharged NVO cathodes in Fig. 3b show no byproducts on the cathode surface in E-0% H_2O, but some ultrathin nanoflakes cover the cathode surface in E-8% H_2O and E-100% H_2O. The X-ray diffraction (XRD) patterns for discharged NVO cathodes in various electrolytes were similar, with no peaks attributed to the ultrathin nanoflakes due to their poor crystallinity, as shown in Fig. 3c. Combined with the findings of previous studies, the ultrathin nanoflakes are layered $Zn_x(OTf)_y(OH)_{2x-y}\cdot nH_2O$ resulting from H^+ insertion.[67] Therefore, the much higher capacity in E-8% H_2O compared to that of E-0% H_2O (Fig. 1a) is mainly attributed to H^+ insertion. Notably, the smaller and thinner flake of $Zn_x(OTf)_y(OH)_{2x-y}\cdot nH_2O$ in E-8% H_2O compared to that in E-100% H_2O indicates better reversibility (appearance and disappearance) during H^+ insertion/extraction (Fig. S13–S15†), indicating better long-term cycling stability.

The X-ray photoelectron spectroscopy (XPS) spectra in Fig. 3d revealed that the Zn^{2+} content in discharged NVO in E-0% H_2O increased compared to that in pristine NVO, directly demonstrating the insertion of Zn^{2+} (but no H^+ insertion due to the absence of protons and $Zn_x(OTf)_y(OH)_{2x-y}\cdot nH_2O$ formation) into NVO. In contrast, Fig. 3d and S16† show that the Zn contents in discharged NVO in E-8% H_2O and E-100% H_2O greatly increased owing to the aggregation of $Zn_x(OTf)_y(OH)_{2x-y}\cdot nH_2O$ on the surface of the discharged cathodes. Concurrently, the binding energy of V decreased, indicating a decrease in the valence state of V, and the intensity of the V-2p

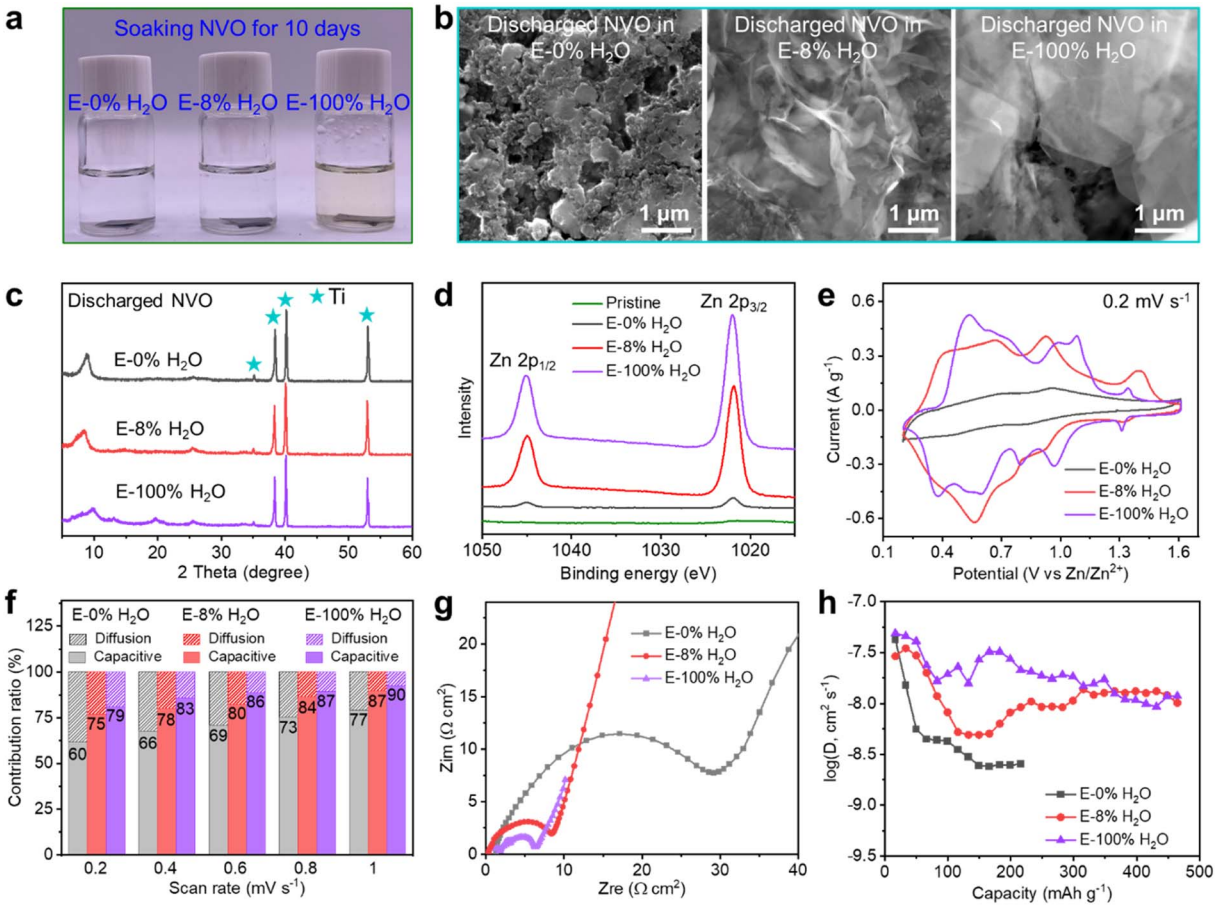

Fig. 3 The effects of water content in the electrolytes on the cathode. (a) Optical images of NVO cathodes in various electrolytes (E-0% H_2O, E-8% H_2O, and E-100% H_2O) after immersion for 10 days. (b) SEM images, (c) XRD patterns and (d) Zn-XPS spectra of the NVO cathode in the discharged state in electrolytes with various water contents. (e) CV curves at 0.2 mV s^{-1} and (f) capacitive contribution ratio at different scan rates from 0.2 to 1 mV s^{-1} for the NVO cathode in electrolytes with various water contents using three electrode cells (WE: NVO cathode; CE: Zn plate; RE: Zn ring). (g) EIS spectra at the OCV state for NVO cathodes using three electrode cells (WE: NVO cathode; CE: Zn plate; RE: Zn ring). (h) The ionic diffusion coefficients of NVO cathodes in electrolytes with various water contents.

XPS peaks declined due to the blocking of $Zn_x(OTf)_y(OH)_{2x-y}\cdot nH_2O$.[24] These results further demonstrated the similar co-insertion of H^+ and Zn^{2+} in E-8% H_2O and E-100% H_2O, which was different from the results obtained with only Zn^{2+} insertion in E-0% H_2O. Therefore, an 8% H_2O content could enable sufficient H^+ insertion, similar to that in a pure aqueous electrolyte (E-100% H_2O).

Although the capacity and H^+-insertion in E-8% H_2O and E-100% H_2O are similar, the distinct CV peaks in Fig. 3e indicate different processes of ion insertion/extraction in E-8% H_2O and E-100% H_2O. The presence of H_2O and AN strongly affects the solvation structure around Zn^{2+}, thus affecting the Zn^{2+}/H^+-insertion kinetics associated with the redox reaction of V. The asymmetrical appearance of the redox peaks in CV is attributed to the reduction/oxidation of V in the cathode materials and the sluggish ion diffusion processes in the cathode materials. Similar complexities have been observed in previous research articles,[15,19,22,74,75] making it challenging to precisely distinguish the specific meaning of each peak. Nevertheless, the changes in the CV shape and area provide valuable information on how electrolytes impact the performance of cathode materials and, consequently, the overall behavior of ZIBs. Fig. 3f and S17† show that the capacitive ratios increase gradually with water content at scan rates ranging from 0.2 to 1 mV s^{-1}, suggesting that water promotes capacitance-type charge transfer.

To investigate the kinetics of Zn^{2+}/H^+ transfer at the cathode/electrolyte interface and in the bulk of the cathode, electrochemical impedance spectroscopy (EIS) and the galvanostatic intermittent titration technique (GITT) were performed. As shown in Fig. 3g, the charge transfer resistances in E-0% H_2O, E-8% H_2O and E-100% H_2O are 28, 8, and 5 Ω cm^2, respectively. The gradual decrease in the charge transfer resistance with increasing water content indicates that water promotes ion-insertion kinetics at the interface. Notably, the ZIBs utilizing the three different electrolytes exhibit remarkably low ohmic resistances (less than 4 Ω cm^2), which lead to a negligible IR drop of approximately 2 mV. This further underscores that the ionic conductivity in this work is sufficiently high to meet the requirements of ZIBs. The GITT results in Fig. 3h and S18† show that the ion coefficients in E-100% H_2O are much higher than

those in E-0% H_2O. In contrast, compared to those in E-100% H_2O, the lower ion coefficients in E-8% H_2O in the middle depth of the discharge (DOD) state indicate dominant Zn^{2+} diffusion, whereas similar coefficients in the high DOD states in E-8% H_2O and E-100% H_2O indicate dominant H^+ diffusion. The results directly demonstrate the critical role of water in ion diffusion processes in the bulk of the cathode. ZIBs typically exhibit much lower ion diffusion coefficients at the cathode than liquid electrolytes. Overall, the water content significantly affects the reversibility, redox processes, charge transfer at the interface and ion transport in the bulk of the cathode. Notably, the charge transfer resistance mainly indicates the kinetics at the interface of the cathode and electrolyte when the battery is in the open circuit voltage (OCV) state. This reflects the insertion ability of ions into the cathodes. However, it should be emphasized that the parameters (including ionic conductivity and charge transfer resistance) do not directly correlate with the capacity and cycling performance of the ZIBs.

The effects of water content on anodes

In addition, the water content in electrolytes also has a significant effect on the static stability and reversibility of Zn stripping/plating. After the Zn plates were immersed in electrolytes with different water contents for 10 days, the Zn surface was smooth and free of byproducts in E-0% H_2O, whereas numerous byproducts covered the Zn surface in E-8% H_2O and E-100% H_2O (Fig. 4a and S19†). Remarkably, the byproducts in E-8% H_2O exhibited a nanoflower morphology comprising ultrathin nanosheets with poor crystallinity, as evidenced by the absence of distinct peaks in the XRD patterns (Fig. 4a). In contrast, the byproducts in E-100% H_2O were nanoplates with a size of approximately 20 μm and exhibited clear XRD peaks corresponding to crystalline $Zn_x(OTf)_y(OH)_{2x-y}\cdot nH_2O$, as shown in Fig. 4a. The pronounced crystallinity of $Zn_x(OTf)_y(OH)_{2x-y}\cdot nH_2O$ has a negative impact on its reversibility, creating significant challenges for the overall performance of the Zn anode. Therefore, reducing the water content in the electrolyte could mitigate the corrosion of Zn, which is favorable for enhancing the static stability.

To investigate the impact of water content on the kinetics of Zn stripping/plating, EIS spectra and galvanostatic polarization curves were recorded in a three-electrode cell with a zinc plate WE, an NVO cathode CE, and a zinc ring RE. At the open circuit voltage (OCV), the EIS spectra (Fig. 4b) reveal that the charge transfer resistances of the Zn foil in E-0% H_2O, E-8% H_2O, and E-100% H_2O are 1500, 145, and 56 Ω cm^{-2}, respectively. The decreasing trend of the charge transfer resistance as the water content in the electrolytes increases indicates that the dissolution and plating processes on the Zn anode become more favorable. This observation is consistent with the well-known fact that Zn is more reactive in H_2O than in AN. These results are also in line with the data presented in Fig. 4c, which show that the initial stripping and plating potentials of Zn in E-0% H_2O are higher than those in E-8% H_2O and E-100% H_2O, indicating faster kinetics in electrolytes that contain water. These findings further demonstrated that water is favorable for fast Zn stripping/plating. The Zn stripping curves in E-8% H_2O and E-100% H_2O exhibit similarities, but the plating potential in E-8% H_2O remains stable, indicating uniform nucleation and growth. In contrast, the plating potential in E-100% H_2O gradually decreases with plating, suggesting that excessive water does not favor uniform plating. Overall, AN-based electrolytes containing 8% water facilitate fast stripping and uniform plating of Zn. Finally, the Zn||Zn symmetric cell in E-8% H_2O exhibited significantly better reversibility than those in E-0% H_2O and E-100% H_2O, as shown in Fig. 4d. Compared to those of E-0% H_2O and E-100% H_2O, the Zn anode had a smoother surface and no byproducts after cycling for 1500 hours (Fig. S20 and S21†), demonstrating the uniqueness of the E-8% H_2O electrolyte.

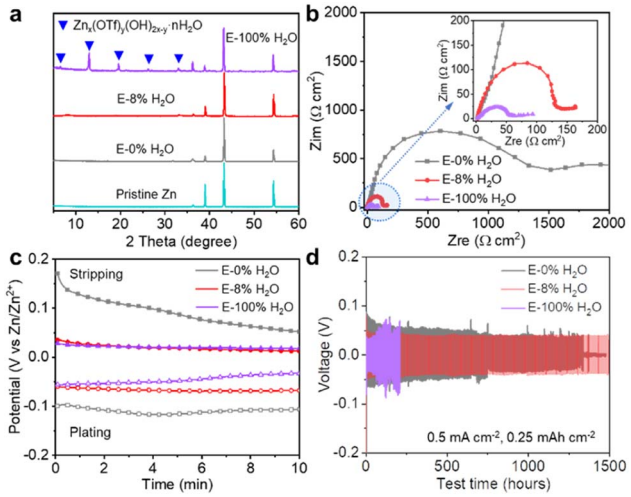

Fig. 4 The effects of electrolytes with various H_2O contents on the Zn anode. (a) XRD patterns of Zn plates in the pristine state and after immersion in various electrolytes (E-0% H_2O, E-8% H_2O and E-100% H_2O) for 10 days. (b) EIS spectra at the OCV state for Zn anodes using the three electrode cells (WE: Zn plate; CE: NVO cathode; RE: Zn ring) in various electrolytes. (c) The polarization curves at 1 mA for Zn stripping/plating in a three electrode cell (WE: Zn plate; CE: NVO cathode; RE: Zn ring) in various electrolytes. The inset shows the enlargement of the blue region. (d) Cycling performance of Zn||Zn symmetric cells at 0.5 mA cm^{-2} with a capacity of 0.25 mA h cm^{-2} in electrolytes with various water contents.

Excellent performance in organic electrolytes with low water content

In brief, while ionic conductivity and charge transfer play crucial roles in ZIBs, their direct relationship with capacity and long-term cycling stability is not straightforward. As demonstrated above, the presence of water in the electrolyte could positively contribute to the capacity, but excessive water can lead to Zn anode corrosion. Striking a balance is essential. Therefore, an electrolyte containing 8% H_2O strikes the right equilibrium by facilitating sufficient H^+-insertion while mitigating water-induced corrosion. This optimum composition allows for the simultaneous achievement of high capacity and excellent stability.

To further demonstrate the benefits of organic solvents with low water content, the rate capability of Zn||NVO using electrolytes with varying water contents was investigated, as depicted in Fig. 5a and S22†. With E-8% H_2O, the discharge capacities are 513, 478, 456, 439, 400, 321, and 233 mA h g^{-1} at 0.1, 0.3, 0.6, 1.0, 2.0, 5.0, and 10.0 A g^{-1}, respectively. Impressively, as the current density ranges from 0.1 A g^{-1} to 10 A g^{-1}, the capacities in E-8% H_2O are higher than those in E-0% H_2O and E-100% H_2O, demonstrating the superior rate capacity in E-8% H_2O. In addition, Fig. 5a also shows 100% capacity recovery in E-8% H_2O after the current density resumes to 0.3 and 0.1 from 10 A g^{-1} excursion, indicating excellent reversibility compared to that in E-100% H_2O. Additionally, Fig. 5b and c demonstrate that Zn||NVO in E-8% H_2O exhibits high reversibility and durability at both low (0.3 A g^{-1}) and high (6 A g^{-1}) rates. Specifically, at 0.3 A g^{-1}, Zn||NVO retains an impressive 94% of its highest capacity after 80 cycles, while at 6 A g^{-1}, it retains 80% of its capacity after 9000 cycles. Similar to the findings at 0.5 A g^{-1} depicted in Fig. 1a, when contrasted with E-8% H_2O, a water content below 8% results in a notable decrease in the specific capacity of the battery, while a water content above 8% leads to a significant deterioration in the cycling stability of the battery (Fig. 5b and S23†). Furthermore, Fig. 5d and S24† show that Zn||NVO in E-8% H_2O has capacities of 500, 360, 313, 233, 172, 134, and 105 mA h g^{-1} at 0.2 A g^{-1} at temperatures of 20, 0, −10, −20, −30, −40, and −50 °C, respectively. E-8% H_2O exhibited superior performance in terms of higher capacity and improved low-temperature operation (0 to −50 °C) compared to E-0% H_2O and E-100% H_2O, possibly attributed to the improved anti-freezing properties. By subjecting electrolytes with different water contents to differential scanning calorimetry (DSC) and temperature cooling tests, it was determined that the E-8% H_2O electrolyte exhibited a lower freezing point (Fig. S25†). Additionally, the photographs in Fig. S26† show that as the temperature decreases from room temperature (20 °C) to −50 °C, crystallization occurs in E-100% H_2O (approximately −20 °C), while $Zn(OTf)_2$ is salted out of the solution in E-0% H_2O (approximately −50 °C) due to the low

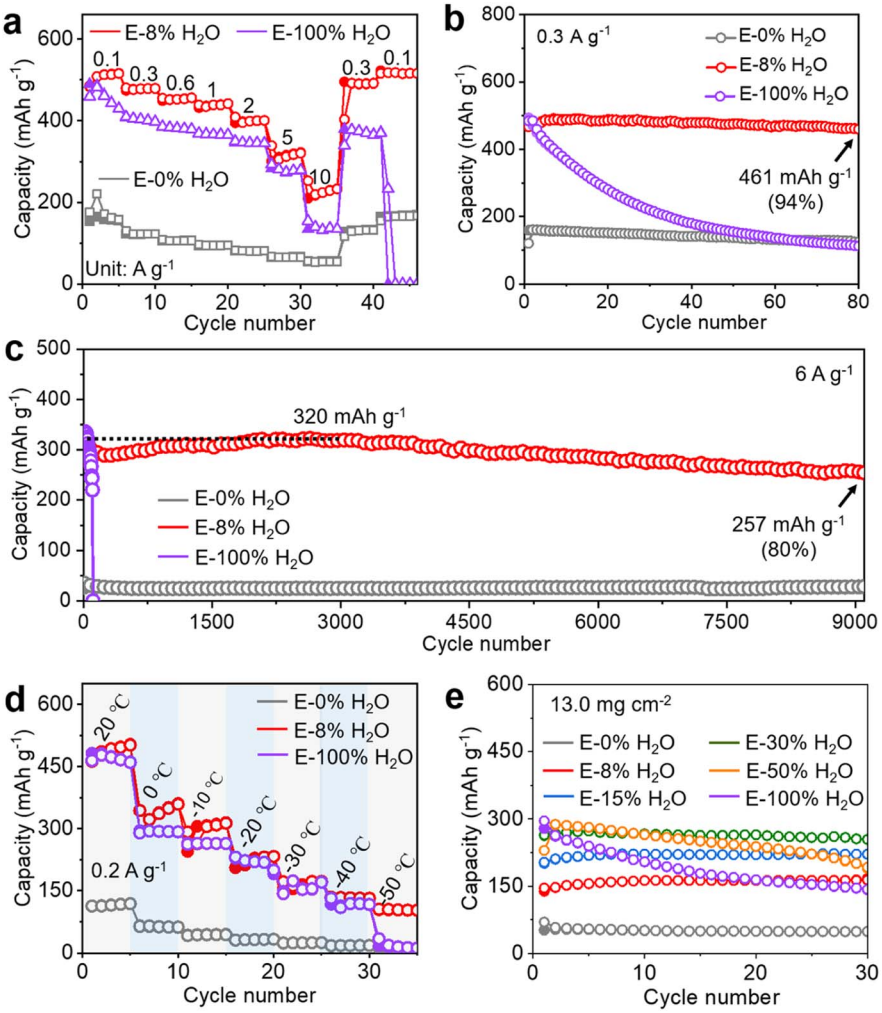

Fig. 5 Electrochemical performance of Zn||NVO in electrolytes with various water contents. (a) Rate performance, (b) cycling performance at a low rate (0.3 A g^{-1}), (c) cycling performance at a high rate (6 A g^{-1}), and (d) performance at various temperatures ranging from 20 to −50 °C for Zn||NVO in electrolytes with various water contents. (e) Cycling performance (specific capacity based on area) at 0.5 A g^{-1} (6.5 mA cm^{-2}) for Zn||NVO with an NVO mass loading of ~13.0 mg cm^{-2} in electrolytes with various water contents.

solubility of $Zn(OTf)_2$ in pure AN. In contrast, E-8% H_2O shows no signs of crystallization or salt-out even at −50 °C. In comparison to those of E-100% H_2O, the heightened anti-freezing properties in both E-0% H_2O and E-8% H_2O can be attributed to the higher anti-freezing properties of acetonitrile relative to water. The enhanced anti-freezing properties in E-8% H_2O, compared to that of E-0% H_2O, are a result of the increased amount of hydrogen bonding between acetonitrile and water (Fig. S27†),[48] as well as the presence of additional components (inducing water molecules). Furthermore, as the temperature decreases to −50 °C, the sharply increased charge transfer resistance (Fig. S28†) indicates a substantial decrease in kinetics, leading to a decrease in capacity. Additionally, there was a pronounced decrease in the ionic conductivities of E-0% H_2O, E-8%H_2O, and E-100%H_2O as the temperature decreased (Fig. S29†). Considering the ionic conductivity, anti-freezing properties, and reaction kinetics, ZIBs in E-8% H_2O demonstrate superior low-temperature performance compared to those in E-0% H_2O and E-100% H_2O.[76]

It is important to highlight that the deliberate variations in the current density shown in Fig. 1a, 5b and d are employed to underscore the universal influence of water content on performance. Despite the variations in current densities, the trends in capacity and stability across varying water contents are similar. Therefore, the utilization of a range of current density tests has enhanced the effectiveness of illustrating the consistent patterns in cycling performance changes.

To demonstrate the applicability of the electrolyte design strategy for potential practical use, Zn||NVO batteries with a cathode mass loading of 13 mg cm^{-2} and a capacity of approximately 3.9 mA h cm^{-2} were systematically studied in 1 M $Zn(OTf)_2$ with various H_2O contents (E-0% H_2O, E-8% H_2O, E-15% H_2O, E-30% H_2O, E-50% H_2O, and E-100% H_2O), as depicted in Fig. 5e and S30.† Since the active mass loading on the cathode may exceed 10 mg cm^{-2} in practical applications, this study aimed to optimize the water content in an electrolyte for high-capacity and stable cycling performance. Interestingly, while E-8% H_2O was found to be the optimal electrolyte for NVO cathodes with a low mass loading of ∼1 mg cm^{-2}, Zn||NVO (13 mg cm^{-2}) in E-30% H_2O achieved the highest capacity and best cycling stability (Fig. 5e and S30†). Given the limited electrolyte volume of 0.1 mL, a higher mass loading necessitates more water molecules, requiring a higher water concentration in the electrolyte to reach the maximum capacity. Therefore, the cathode mass loading significantly influences the optimal water concentration in the electrolyte for achieving high capacity and cycling stability concurrently. The optimal water content increases from 8% to 30% with an increase in mass loading from ∼1 mg cm^{-2} to ∼13 mg cm^{-2}. Careful tuning of the water content in the electrolyte is essential to strike the right balance.

The primary objective of this study is to emphasize the impact of the water content in electrolytes on the performance (including capacity and stability) of ZIBs, rather than asserting that the $Zn(OTf)_2$/AN/H_2O electrolyte is superior to other electrolytes. Fundamentally, we demonstrate that even a small amount of water plays a crucial role in enhancing the capacity of ZIBs.

Notably, in an anhydrous electrolyte, zinc-ion batteries exhibit a significantly low capacity (∼110 mA h g^{-1}), which falls far below the theoretical capacity (536 mA h g^{-1}). This is attributed to the sole insertion of Zn^{2+} and sluggish kinetics. Introducing water into the electrolyte facilitates proton intercalation, thereby enhancing the battery capacity. In the initial state, a higher availability of H^+ allows for increased capacity, consequently yielding a capacity boost with increasing water content in the electrolyte. However, when the water content reaches the requirement for the highest capacity, an excess of water contributes to a decrease in cycling stability for the following three main reasons. First, in the positive electrode, dissolution triggered by water results in the formation of the by-product $Zn_3(OH)_2V_2O_7\cdot 2H_2O$ in vanadium-based materials. Second, the irreversible generation of alkaline zinc salts due to proton intercalation in aqueous electrolytes can diminish battery stability. Third, water also results in hydrogen evolution and the formation of basic zinc salts on the Zn anode. Therefore, maintaining an optimal electrolyte water content is crucial for simultaneously achieving a high capacity through proton intercalation and preventing side reactions caused by excess water.

From a practical standpoint, our electrolyte design strategy holds potential for universal application in other hybrid electrolyte solutions, making it versatile and applicable to various battery systems. This work showcases the broad applicability of our findings and their potential contribution to advancing battery technology. Furthermore, this study adeptly demonstrated the immediate impact of water content and the specific organic solvent type within the electrolyte on both the anode and cathode, consequently exerting a significant influence on capacity and cycling performance. When fine-tuning the electrolyte composition, a comprehensive assessment of the effects on both the anode and cathode becomes paramount, transcending a singular emphasis on either the anode or cathode results.

Conclusions

To summarize, our study successfully demonstrated that organic solvents with low water content can simultaneously achieve high capacity, high rate-capability, and excellent cycling stability. The small amount of water in the electrolyte allows sufficient H^+-insertion while mitigating corrosion and electrode dissolution. Additionally, the water content strongly affects the solvation structure around Zn^{2+}, thereby affecting the reversibility of the $Zn_x(OTf)_y(OH)_{2x-y}\cdot nH_2O$ byproducts resulting from H^+-insertion. Moreover, the water content in the electrolyte affects the kinetics and reversibility of Zn stripping/plating at the anode and ion insertion/extraction at the cathode. Our experiments in a $Zn(OTf)_2$ electrolyte using 8% H_2O in AN as the solvent demonstrated that Zn||NVO achieved a capacity as high as 475 mA h g^{-1} at 0.5 A g^{-1}, with a capacity retention of 92% after 100 cycles. The capacity retention was 80% of the highest capacity at 6 A g^{-1} after 9000 cycles. This is the first report showing that only a small amount of water (8%, v/v) in an electrolyte can achieve both a high capacity, akin to that of pure aqueous electrolytes, and a long cycle-life, comparable to that of

organic electrolytes. Additionally, compared to electrolytes using pure water and AN solvents, Zn||NVO in the $Zn(OTf)_2$ electrolyte using 8% H_2O in AN as the solvent had a higher capacity at low temperatures ranging from 0 to −50 °C, indicating better anti-freezing properties. Furthermore, we demonstrated that the optimal water content in the electrolyte is dependent on the mass loading with solid evidence of a cathode with high mass loading (up to 13 mg cm^{-2}), demonstrating the applicability of the electrolyte design strategy for potential practical use. Overall, the design strategy of tuning the water content in the electrolyte can effectively eliminate the trade-off between capacity and cycling stability, providing a new possibility for constructing high-performance commercial ZIBs.

Data availability

Experimental and computational data is available upon request to the corresponding authors.

Author contributions

W. Y., K. Z. and W. J. conceived and designed this work. K. Z. and W. J. collected and analysed the data. W. X. Z. W., and Z. O. assisted with the material synthesis and characterization. K. Z. and W. J. wrote the article. W. Y. revised the article and supervised the project. All the authors contributed to the discussion of the results.

Conflicts of interest

There are no conflicts to declare.

Acknowledgements

All the authors appreciate the financial support from the Youth Innovation Fund of the Dalian Institute of Chemical Physics (DICP I202126) and the project from Liaoning Province (2023-MS-014).

References

1 C. Yang, J. Xia, C. Cui, T. P. Pollard, J. Vatamanu, A. Faraone, J. A. Dura, M. Tyagi, A. Kattan, E. Thimsen, J. Xu, W. Song, E. Hu, X. Ji, S. Hou, X. Zhang, M. S. Ding, S. Hwang, D. Su, Y. Ren, X.-Q. Yang, H. Wang, O. Borodin and C. Wang, *Nat. Sustain.*, 2023, **6**, 325–335.
2 D. Han, C. Cui, K. Zhang, Z. Wang, J. Gao, Y. Guo, Z. Zhang, S. Wu, L. Yin, Z. Weng, F. Kang and Q.-H. Yang, *Nat. Sustain.*, 2022, **5**, 205–213.
3 C. Li, S. Jin, L. A. Archer and L. F. Nazar, *Joule*, 2022, **6**, 1733–1738.
4 L. E. Blanc, D. Kundu and L. F. Nazar, *Joule*, 2020, **4**, 771–799.
5 J. Zhou, L. Shan, Z. Wu, X. Guo, G. Fang and S. Liang, *Chem. Commun.*, 2018, **54**, 4457–4460.
6 M. Kar and C. Pozo-Gonzalo, *Curr. Opin. Green Sustain. Chem.*, 2021, **28**, 100426.
7 M. Yan, P. He, Y. Chen, S. Wang, Q. Wei, K. Zhao, X. Xu, Q. An, Y. Shuang, Y. Shao, K. T. Mueller, L. Mai, J. Liu and J. Yang, *Adv. Mater.*, 2018, **30**, 1703725.
8 D. Kundu, S. Hosseini Vajargah, L. Wan, B. Adams, D. Prendergast and L. F. Nazar, *Energy Environ. Sci.*, 2018, **11**, 881–892.
9 Y. Lv, Y. Xiao, L. Ma, C. Zhi and S. Chen, *Adv. Mater.*, 2022, **34**, 2106409.
10 A. Naveed, H. Yang, Y. Shao, J. Yang, N. Yanna, J. Liu, S. Shi, L. Zhang, A. Ye, B. He and J. Wang, *Adv. Mater.*, 2019, **31**, 1900668.
11 F. Wang, W. Sun, Z. Shadike, E. Hu, X. Ji, T. Gao, X. Q. Yang, K. Xu and C. Wang, *Angew. Chem., Int. Ed.*, 2018, **57**, 11978–11981.
12 X. Qiu, N. Wang, Z. Wang, F. Wang and Y. Wang, *Angew. Chem., Int. Ed.*, 2021, **60**, 9610–9617.
13 S. D. Han, N. N. Rajput, X. Qu, B. Pan, M. He, M. S. Ferrandon, C. Liao, K. A. Persson and A. K. Burrell, *ACS Appl. Mater. Interfaces*, 2016, **8**, 3021–3031.
14 M. Li, Z. Li, X. Wang, J. Meng, X. Liu, B. Wu, C. Han and L. Mai, *Energy Environ. Sci.*, 2021, **14**, 3796–3839.
15 K. Zhu, T. Wu, W. van den Bergh, M. Stefik and K. Huang, *ACS Nano*, 2021, **15**, 10678–10688.
16 K. Zhu, W. Jiang, Z. Wang, W. Li, W. Xie, H. Yang and W. Yang, *Angew. Chem., Int. Ed.*, 2023, **62**, e202213368.
17 T. Wu, K. Zhu, C. Qin and K. Huang, *J. Mater. Chem. A*, 2019, **7**, 5612–5620.
18 Q. Sun, H. Cheng, Y. Yuan, Y. Liu, W. Nie, K. Zhao, K. Wang, W. Yao, X. Lu and J. Lu, *Adv. Energy Mater.*, 2023, **13**, 2202515.
19 D. Kundu, B. D. Adams, V. Duffort, S. H. Vajargah and L. F. Nazar, *Nat. Energy*, 2016, **1**, 16119.
20 K. Zhu, T. Wu and K. Huang, *ACS Nano*, 2019, **13**, 14447.
21 H. Pan, Y. Shao, P. Yan, Y. Cheng, K. S. Han, Z. Nie, C. Wang, J. Yang, X. Li, P. Bhattacharya, K. T. Mueller and J. Liu, *Nat. Energy*, 2016, **1**, 16039.
22 F. Wan, L. Zhang, X. Dai, X. Wang, Z. Niu and J. Chen, *Nat. Commun.*, 2018, **9**, 1656.
23 F. Yue, Z. Tie, Y. Zhang, S. Bi, Y. Wang and Z. Niu, *Angew. Chem., Int. Ed.*, 2022, **61**, e202208513.
24 K. Zhu, T. Wu, S. Sun, W. van den Bergh, M. Stefik and K. Huang, *Energy Storage Mater.*, 2020, **29**, 60–70.
25 W. Sun, F. Wang, S. Hou, C. Yang, X. Fan, Z. Ma, T. Gao, F. Han, R. Hu, M. Zhu and C. Wang, *J. Am. Chem. Soc.*, 2017, **139**, 9775–9778.
26 N. Zhang, X. Chen, M. Yu, Z. Niu, F. Cheng and J. Chen, *Chem. Soc. Rev.*, 2020, **49**, 4203–4219.
27 X. Jia, C. Liu, Z. G. Neale, J. Yang and G. Cao, *Chem. Rev.*, 2020, **120**, 7795–7866.
28 B. Tang, L. Shan, S. Liang and J. Zhou, *Energy Environ. Sci.*, 2019, **12**, 3288–3304.
29 J. Huang, Z. Wang, M. Hou, X. Dong, Y. Liu, Y. Wang and Y. Xia, *Nat. Commun.*, 2018, **9**, 2906.
30 H. Yang, T. Zhang, D. Chen, Y. Tan, W. Zhou, L. Li, W. Li, G. Li, W. Han, H. J. Fan and D. Chao, *Adv. Mater.*, 2023, **35**, 2300053.

31 Z. Tie, L. Liu, S. Deng, D. Zhao and Z. Niu, *Angew. Chem., Int. Ed.*, 2020, **59**, 4920–4924.
32 Q. Zhao, W. Huang, Z. Luo, L. Liu, Y. Lu, Y. Li, L. Li, J. Hu, H. Ma and J. Chen, *Sci. Adv.*, 2018, **4**, eaao1761.
33 L. Zhang, L. Chen, X. Zhou and Z. Liu, *Adv. Energy Mater.*, 2015, **5**, 1400930.
34 Z. Tie and Z. Niu, *Angew. Chem., Int. Ed.*, 2020, **59**, 21293–21303.
35 F. Wan and Z. Niu, *Angew. Chem., Int. Ed.*, 2019, **58**, 16358–16367.
36 Y. Liu and X. Wu, *J. Energy Chem.*, 2021, **56**, 223–237.
37 S. Zhang, H. Tan, X. Rui and Y. Yu, *Acc. Chem. Res.*, 2020, **53**, 1660–1671.
38 H. Jiang, Y. Zhang, Z. Pan, L. Xu, J. Zheng, Z. Gao, T. Hu and C. Meng, *Electrochim. Acta*, 2020, **332**, 135506.
39 D. Bin, Y. Liu, B. Yang, J. Huang, X. Dong, X. Zhang, Y. Wang and Y. Xia, *ACS Appl. Mater. Interfaces*, 2019, **11**, 20796–20803.
40 Q. Li, X. Rui, D. Chen, Y. Feng, N. Xiao, L. Gan, Q. Zhang, Y. Yu and S. Huang, *Nanomicro Lett.*, 2020, **12**, 67.
41 P. Hu, T. Zhu, X. Wang, X. Wei, M. Yan, J. Li, W. Luo, W. Yang, W. Zhang, L. Zhou, Z. Zhou and L. Mai, *Nano Lett.*, 2018, **18**, 1758–1763.
42 V. Soundharrajan, B. Sambandam, S. Kim, M. H. Alfaruqi, D. Y. Putro, J. Jo, S. Kim, V. Mathew, Y. K. Sun and J. Kim, *Nano Lett.*, 2018, **18**, 2402–2410.
43 Y. Zhang, X. Zheng, N. Wang, W.-H. Lai, Y. Liu, S.-L. Chou, H.-K. Liu, S.-X. Dou and Y.-X. Wang, *Chem. Sci.*, 2022, **13**, 14246–14263.
44 K. Zhu, T. Wu and K. Huang, *Chem. Mater.*, 2021, **33**, 4089–4098.
45 K. Zhu, T. Wu and K. Huang, *Energy Storage Mater.*, 2021, **38**, 473–481.
46 F. Ming, Y. Zhu, G. Huang, A. H. Emwas, H. Liang, Y. Cui and H. N. Alshareef, *J. Am. Chem. Soc.*, 2022, **144**, 7160–7170.
47 W. Yang, X. Du, J. Zhao, Z. Chen, J. Li, J. Xie, Y. Zhang, Z. Cui, Q. Kong, Z. Zhao, C. Wang, Q. Zhang and G. Cui, *Joule*, 2020, **4**, 1557–1574.
48 W. Chen, S. Guo, L. Qin, L. Li, X. Cao, J. Zhou, Z. Luo, G. Fang and S. Liang, *Adv. Funct. Mater.*, 2022, **32**, 2112609.
49 Y. Chen, S. Guo, L. Qin, Q. Wan, Y. Pan, M. Zhou, M. Long, G. Fang and S. Liang, *Batteries Supercaps*, 2022, **5**, e202200001.
50 F. Wang, O. Borodin, T. Gao, X. Fan, W. Sun, F. Han, A. Faraone, J. A. Dura, K. Xu and C. Wang, *Nat. Mater.*, 2018, **17**, 543–549.
51 R. Wang, M. Yao, M. Yang, J. Zhu, J. Chen and Z. Niu, *Proc. Natl. Acad. Sci. U. S. A.*, 2023, **120**, e2221980120.
52 C. Zhang, J. Holoubek, X. Wu, A. Daniyar, L. Zhu, C. Chen, D. P. Leonard, I. A. Rodriguez-Perez, J. X. Jiang, C. Fang and X. Ji, *Chem. Commun.*, 2018, **54**, 14097–14099.
53 X. Wu, Y. Xu, C. Zhang, D. P. Leonard, A. Markir, J. Lu and X. Ji, *J. Am. Chem. Soc.*, 2019, **141**, 6338–6344.
54 L. Zhang, I. A. Rodríguez-Pérez, H. Jiang, C. Zhang, D. P. Leonard, Q. Guo, W. Wang, S. Han, L. Wang and X. Ji, *Adv. Funct. Mater.*, 2019, **29**, 1902653.
55 S. Huang, J. Zhu, J. Tian and Z. Niu, *Chem. Eur. J.*, 2019, **25**, 14480–14494.
56 Z. Zhang, Z. He, N. Wang, F. Wang, C. Du, J. Ruan, Q. Li, D. Sun, F. Fang and F. Wang, *Adv. Funct. Mater.*, 2023, **33**, 2214648.
57 J. Shi, K. Xia, L. Liu, C. Liu, Q. Zhang, L. Li, X. Zhou, J. Liang and Z. Tao, *Electrochim. Acta*, 2020, **358**, 136937.
58 C. Li, X. Xie, S. Liang and J. Zhou, *Energy Environ. Mater.*, 2020, **3**, 146–159.
59 L. Ma, J. Vatamanu, N. T. Hahn, T. P. Pollard, O. Borodin, V. Petkov, M. A. Schroeder, Y. Ren, M. S. Ding, C. Luo, J. L. Allen, C. Wang and K. Xu, *Proc. Natl. Acad. Sci. U. S. A.*, 2022, **119**, e2121138119.
60 L. Cao, D. Li, E. Hu, J. Xu, T. Deng, L. Ma, Y. Wang, X.-Q. Yang and C. Wang, *J. Am. Chem. Soc.*, 2020, **142**, 21404–21409.
61 Q. Zhang, J. Luan, L. Fu, S. Wu, Y. Tang, X. Ji and H. Wang, *Angew. Chem., Int. Ed.*, 2019, **58**, 15841–15847.
62 T. C. Li, Y. Lim, X. L. Li, S. Luo, C. Lin, D. Fang, S. Xia, Y. Wang and H. Y. Yang, *Adv. Energy Mater.*, 2022, **12**, 2103231.
63 K. Zhu, T. Wu, S. Sun, Y. Wen and K. Huang, *ChemElectroChem*, 2020, **7**, 2714–2735.
64 L. Yuan, J. Hao, C.-C. Kao, C. Wu, H.-K. Liu, S.-X. Dou and S.-Z. Qiao, *Energy Environ. Sci.*, 2021, **14**, 5669–5689.
65 Y. Wang, Z. Wang, F. Yang, S. Liu, S. Zhang, J. Mao and Z. Guo, *Small*, 2022, **18**, e2107033.
66 Z. Hou, H. Tan, Y. Gao, M. Li, Z. Lu and B. Zhang, *J. Mater. Chem. A*, 2020, **8**, 19367–19374.
67 P. Oberholzer, E. Tervoort, A. Bouzid, A. Pasquarello and D. Kundu, *ACS Appl. Mater. Interfaces*, 2019, **11**, 674–682.
68 H.-C. Zhou, X.-L. Li, J.-L. Liu, C. Peng, B. Zhang, J. Chen, Q. Su, L. Wu and Y.-Z. Yuan, *Chem. Pap.*, 2015, **69**, 1361–1366.
69 J. C. Yang, M. J. Jablonsky and J. W. Mays, *Polymer*, 2002, **43**, 5125–5132.
70 N. Chang, T. Li, R. Li, S. Wang, Y. Yin, H. Zhang and X. Li, *Energy Environ. Sci.*, 2020, **13**, 3527–3535.
71 J. Niu, X. You, C. Duan, H. Fun and Z. Zhou, *Inorg. Chem.*, 1996, **35**, 4211–4217.
72 Y. Zhang, G. Wan, N. H. C. Lewis, J. Mars, S. Bone, H.-G. Steinrück, M. R. Lukatskaya, N. J. Weadock, M. Bajdich, O. Borodin, A. Tokmakoff, M. F. Toney and E. J. Maginn, *ACS Energy Lett.*, 2022, **7**, 1694–1695.
73 R. A. Mowery, *J. Chromatogr. Sci.*, 1985, **23**, 22–29.
74 C. Xia, J. Guo, P. Li, X. Zhang and H. N. Alshareef, *Angew. Chem., Int. Ed.*, 2018, **57**, 3943–3948.
75 R. Chen, C. Zhang, J. Li, Z. Du, F. Guo, W. Zhang, Y. Dai, W. Zong, X. Gao, J. Zhu, Y. Zhao, X. Wang and G. He, *Energy Environ. Sci.*, 2023, **16**, 2540–2549.
76 Z. Liu, X. Luo, L. Qin, G. Fang and S. Liang, *Adv. Powder Mater.*, 2022, **1**, 100011.